Spin flop transition in doped antiferromagnets

2003 J. Phys.: Condens. Matter 15 7271

(http://iopscience.iop.org/0953-8984/15/43/011)

INSTITUTE OF PHYSICS PUBLISHING JOURNAL OF PHYSICS: CONDENSED MATTER

J. Phys.: Condens. Matter **15** (2003) 7271–7286 PII: S0953-8984(03)63808-7

Spin flop transition in doped antiferromagnets

N M R Peres

Departamento de Física and GCEP-Centro de Física da Universidade do Minho, Campus Gualtar, P-4700-320 Braga, Portugal

Received 22 May 2003
Published 17 October 2003
Online at stacks.iop.org/JPhysCM/15/7271

Abstract

In this paper we compute the mean field phase diagram of a doped antiferromagnet, in a magnetic field and with anisotropic exchange. We show that at zero temperature there is a metamagnetic transition from the antiferromagnetic configuration along the z direction to a spin flop (SF) state. In the spin flop phase the system prefers a commensurate magnetic order, at low doping, whereas at larger doping the incommensurate phase is favourable. Contrary to the pure Heisenberg case, the spin flop region does not span an infinite area in the (Δ, h) plane, where Δ is the exchange anisotropy and h is the external magnetic field. We characterize the magnetic and charge-transport properties of the SF phase, computing the magnetic susceptibility and the Drude weight. This latter quantity presents a sudden variation as the SF to paramagnet phase transition line is crossed. This effect could be used as a possible source of large magnetoresistance. Our findings may have some relevance for doped $La_{2-\delta}Sr_{\delta}CuO_4$ in a magnetic field.

(Some figures in this article are in colour only in the electronic version)

1. Introduction

Metamagnetic transitions are ubiquitous in nature. We can find them in pure magnets, in boson systems, in spin density wave systems, and in doped antiferromagnets.

When placed in a magnetic field many magnetic materials undergo first-order phase transitions. These materials are called metamagnets. Two of the best studied magnetic materials exhibiting metamagnetic transitions are MnF_2 and $FeCl_2$ [1–3]. In $FeCl_2$ there is a first-order transition from an antiferromagnetic (AF) to a paramagnetic (P) state, and in MnF_2 there is a first-order transition from an AF to a spin flop (SF) state (see figure 1, panel (a), for a schematic idea on the spin configurations). In addition to the metamagnetic transitions mentioned above, these materials also undergo second-order phase transitions. The way the second- and first-order transition lines touch each other introduces different types of critical points. In MnF_2 and $FeCl_2$ there is a bicritical and a tricritical point, respectively. Some materials, such as $GdAlO_3$ [4], can present different types of critical points depending on the orientation of the magnetic field.

0953-8984/03/437271+16$30.00

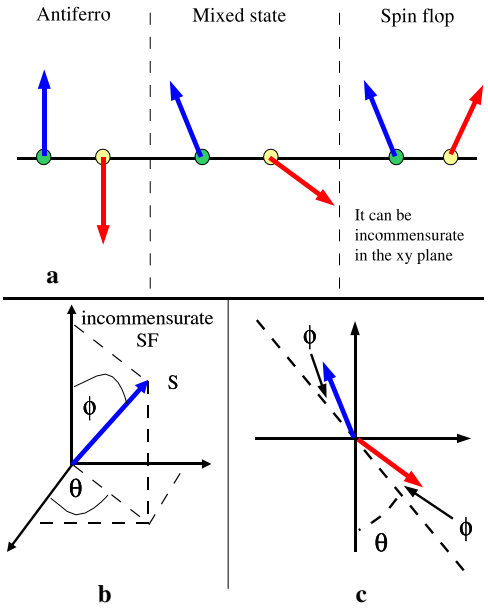

Figure 1. Panel (a): schematic arrangement of the spin on the two sub-lattices in the AF, mixed, and SF states. Panel (b): definition of the angles for the spins in the spin flop incommensurate spiral state given by equation (3). Panel (c): definitions of the angles for the spins, including the AF, the SF, and the mixed states. The letters S_A and S_B denote the spins on sub-lattices A and B respectively. The spin configuration refers to the commensurate states given by equation (2).

From a theoretical point of view, and as early as 1936, Néel [5] predicted a first-order magnetic transition for an anisotropic antiferromagnet in a magnetic field. This metamagnetic transition was named the SF transition. Improvements of Néel's results were achieved using Green functions and Holstein–Primakov bosons [6, 7]. Later, a scaling theory for bicritical points, based on a renormalization group analysis, was introduced [8]. More recently, a zero-temperature SF transition in square and cubic lattices was studied, using exact diagonalization [9], and the SSE Monte Carlo method [10]. The finite temperature study of the model phase diagram, using exact (numerical) methods, was done recently, but for the two-dimensional case only, and in the context of hard core bosons [11]. (The three-dimensional case, at finite temperatures, was also studied [12].)

The exact mapping between hard-core bosons with nearest neighbour interaction and the spin $1/2$ anisotropic Heisenberg model [13], permits us to obtain results for both physical systems from the study of one of them alone [14]. In the boson language, the AF and spin flop phases correspond to a Mott insulator phase (a solid phase), where the bosons are locked at the lattice sites by the nearest neighbour repulsion, and to the super-fluid phase, respectively. The observation of the Mott insulator to super-fluid transition (and vice versa) in a Bose–Einstein condensate of ^{87}Rb atoms confined by an optical trap [15] gave an enormous boost to the research, both theoretical and experimental, in this field [16]. The effect of disorder in the phase diagram of the two-dimensional boson–Hubbard system has been studied as well [17].

Also in doped magnetic materials, such as in $La_{2-\delta}Sr_{\delta}CuO_4$, metamagnetic transitions have been observed [19]. Both in pure La_2CuO_4 and in lightly doped $La_{2-\delta}Sr_{\delta}CuO_4$ the spin flop transition has its origin in the Dzyaloshinskii–Moriya interaction. Although some theoretical study of this transition has been done in the past for pure La_2CuO_4 [20], its study

in doped $La_{2-\delta}Sr_{\delta}CuO_4$ has not been pursued to our knowledge. The spin wave spectrum for doped La_2CuO_4 was considered by Ivanov *et al* [21]. The interesting magnetic properties of $La_{2-\delta}Sr_{\delta}CuO_2$ motivated us to carry out general studies of metamagnetic transitions in anisotropic doped antiferromagnets. To the best of our knowledge, the only work dealing with metamagnetic transitions in strongly correlated electrons was done in the context of the Hubbard model [22].

The paper is organized as follows. In section 2, we introduce the model and the possible spin phases that may exist in the system; in section 3, the zero- and finite-temperature phase-diagrams of the system are introduced and discussed, together with the effect of doping on the critical fields and on the SF angle; in section 4 the metallic SF phase is characterized both in terms of its magnetic and transport properties.

2. Model and mean field equations

Our starting point is a simple generalization of the usual t–t'–J model in three dimensions, where an anisotropic exchange term, of strength $J\Delta$, in included

$$H = -\frac{t}{2}\sum_{i,\beta,\sigma}(c^{\dagger}_{i,\sigma}c_{i+\beta,\sigma} + \text{h.c.}) - \frac{t'}{2}\sum_{i,\beta',\sigma}(c^{\dagger}_{i,\sigma}c_{i+\beta',\sigma} + \text{h.c.}) + \frac{J}{2}\sum_{i,\beta}(\Delta S^z_i S^z_{i+\beta} + S^x_i S^x_{i+\beta} + S^y_i S^y_{i+\beta}) - h\sum_i S^z_i - \mu\sum_{i,\sigma}c^{\dagger}_{i,\sigma}c_{i,\sigma}. \quad (1)$$

In the Hamiltonian (1), β and β' stand for the lattice vectors connecting all nearest and second-nearest neighbours sites of site i in a 3D cubic lattice, respectively; the parameters t and t' stand for the hopping integrals connecting all nearest and second-nearest neighbours sites, respectively, h stands for the magnetic field and μ for the chemical potential. The density of electrons is defined as $n = N_e/N$, where N_e is the total number of electrons and N is the number of lattice sites. Since our calculations will be performed at electronic densities close to $n = 1$ it is convenient for later use to introduce the doping of holes as $\delta = 1 - n \ll 1$.

It is a characteristic of t–J models (we are referring here to class of models) that only one electron at the most can exist at each lattice site. We enforce this constraint using a slave boson representation for the $c_{i,\sigma}$ operators [23]. In this representation we have $c_{i,\sigma} = b^{\dagger}_i f_{i,\sigma}$ and $\vec{S} = \frac{1}{2}\sum_{\alpha',\alpha} f^{\dagger}_{i,\alpha}\vec{\sigma}_{\alpha',\alpha}f_{i,\alpha'}$, where $\vec{\sigma} = (\sigma_x, \sigma_y, \sigma_z)$ are the usual Pauli matrices. At each lattice site the total number of bosons and fermions is equal to one, and we have the constraint $\sum_{\sigma} f^{\dagger}_{i,\sigma}f_{i,\sigma} + b^{\dagger}_i b_i = 1$. In what follows, we shall consider that all bosons have condensed into the lowest energy state, and introduce $\langle b\rangle = \sqrt{\delta}$, where δ corresponds, for zero and moderate temperatures (see finite temperature discussion), to the doping introduced above.

In order to introduce a mean field Hamiltonian suitable for the study of metamagnetic transitions we consider two sub-lattices, A and B, such that in each sub-lattice the spins are oriented as shown in figure 1, panel (c). Referring to figure 1, panel (c), $\theta = \phi = 0$ describes the AF configuration; $\theta = \pi/2$ and $\phi \neq 0$ describes the SF configuration; $\theta = \pi/2$ and $\phi = \pi/2$ describes the P configuration (the term 'P configuration' to name a state where both spins point up may cause some confusion, but in this context it means the system does not present a ferromagnetic ground state, this is, it does not possess a ferromagnetic order parameter, in the sense of Landau theory of phase transitions; the magnetic moment presented by the system is induced by the magnetic field); $\theta \neq 0$ and $\phi \neq 0$ corresponds to a mixed phase, where there is staggered magnetization in both the z and y directions. The spin averages

of all these configurations, in sub-lattices A and B, are given by

$$\begin{aligned}\langle\vec{S}_{i_A}\rangle &= (0, -S_A\sin(\theta-\phi), S_A\cos(\theta-\phi)),\\ \langle\vec{S}_{i_B}\rangle &= (0, S_B\sin(\theta+\phi), -S_B\cos(\theta+\phi)).\end{aligned} \tag{2}$$

Note that we consider the magnitude of the average value of the spin to be different at the two sub-lattices. This is needed because the magnetic field induces a certain amount of ferrimagnetism in the system. The above phases are commensurate with the lattice, but it is well known that the isotropic t–J model supports spiral order in the xy plane with a momentum vector $\vec{Q}$ incommensurate with the lattice [18]. To account for this possibility in the presence of a magnetic field, we introduce averages of the spin operators, presenting spiral order in the xy plane

$$\langle\vec{S}_i\rangle = S(\sin\phi\cos\theta_i, \sin\phi\sin\theta_i, \cos\phi), \tag{3}$$

where $\theta_i = \vec{Q}\cdot\vec{R}_i$, and ϕ represents the angle of $\vec{S}$ with the z axis (see figure 1, panel (b)). This phase competes with the commensurate SF order. It is also possible that the commensurate AF order in the z direction may compete with an AF order presenting incommensurate spiral order in the xy plane

$$\langle\vec{S}_{i_A}\rangle = S_A(\sin\phi_A\cos\theta_i, \sin\phi_A\sin\theta_i, \cos\phi_A), \tag{4}$$

$$\langle\vec{S}_{i_B}\rangle = S_B(\sin\phi_B\cos\theta_i, \sin\phi_B\sin\theta_i, -\cos\phi_B). \tag{5}$$

In our study we have not found solutions for the mixed state and for the AF order presenting incommensurate spiral order in the xy plane.

2.1. Commensurate AF and SF phases

Using the averages (2) and introducing a Hartree–Fock decoupling of the Hamiltonian (1) we obtain, after Fourier transforming the operators, the following mean field Hamiltonian

$$\begin{aligned}H_{\mathrm{MF}} = &\sum_{k,\sigma}\epsilon_1(k)(a^\dagger_{k,\sigma}b_{k,\sigma} + b^\dagger_{k,\sigma}a_{k,\sigma}) + \sum_{k,\sigma}[\epsilon_2(k)+\sigma h^z_B]a^\dagger_{k,\sigma}a_{k,\sigma}\\ &+ \sum_{k,\sigma}[\epsilon_2(k)+\sigma h^z_A]b^\dagger_{k,\sigma}b_{k,\sigma} + \sum_{k,\sigma}h^x_B a^\dagger_{k,\sigma}a_{k,-\sigma} + \sum_{k,\sigma}h^x_A b^\dagger_{k,\sigma}b_{k,-\sigma}\end{aligned} \tag{6}$$

where the $a^\dagger_{k,\sigma}$ and the $b^\dagger_{k,\sigma}$ operators refer to the sub-lattices A and B, respectively, k stands for $\vec{k}$, the k summation runs over the magnetic Brillouin zone, and

$$\epsilon_1(k) = -2t\delta\sum_{i=x,y,z}\cos k_i, \qquad \epsilon_2(k) = -4t'\delta\sum_{j\neq i=x,y,z}\cos k_i\cos k_j,$$

$$h^z_{A/B} = 3J\Delta\langle S^z_{A/B}\rangle - \frac{h}{2}, \qquad h^x_{A/B} = 3J\langle S^x_{A/B}\rangle.$$

We point out that in $\epsilon_1(k)$ and $\epsilon_2(k)$ the condensation of the bosons renormalizes the hopping integrals to $t\delta$ and $t'\delta$. Since we assumed the condensation of the bosons, the constraint $\left(\sum_\sigma f^\dagger_{i,\sigma}f_{i,\sigma} + b^\dagger_i b_i = 1\right)$ gives an equation for the number of particles in terms of the doping δ

$$\frac{1}{N}\sum_{k,\sigma}(\langle a^\dagger_{k,\sigma}a_{k,\sigma}\rangle + \langle b^\dagger_{k,\sigma}b_{k,\sigma}\rangle) = 1-\delta. \tag{7}$$

In the P phase there is one mean field parameter only: the average value of the spin $S = S_A = S_B$; in the AF and SF phases we have the mean field parameters S_A and S_B, and S and ϕ, respectively. All physical quantities characterizing model (6) can be obtained from the associated single particle Green functions.

2.2. *Incommensurate (spiral) SF phase*

Considering the SF incommensurate states given by (3), the mean field Hamiltonian can be cast in the form

$$H = \sum_k [\epsilon_\uparrow(k+Q) f^\dagger_{k+Q,\uparrow} f_{k+Q,\uparrow} + \epsilon_\downarrow(k) f^\dagger_{k,\downarrow} f_{k,\downarrow}] + \bar{\Delta} \sum_k (f^\dagger_{k+Q,\uparrow} f_{k,\downarrow} + f^\dagger_{k,\downarrow} f_{k+Q,\uparrow}) + E_0, \tag{8}$$

where

$$\begin{aligned}
&\epsilon_\uparrow(k+Q) = \epsilon_1(k+Q) + \epsilon_2(k+Q) + h_z - \mu,\\
&h_z = -\frac{h}{2} + \frac{J}{2}\Delta S \cos\phi z,\\
&\epsilon_\downarrow(k) = \epsilon_1(k) + \epsilon_2(k) - h_z - \mu,\\
&\bar{\Delta} = \frac{J}{2} S \sin\phi \gamma(Q),\\
&\gamma(k) = 2 \sum_{i=x,y,z} \cos(k_i),\\
&E_0 = -\frac{J}{2}\Delta S^2 \cos^2\phi z N - \frac{J}{2} S^2 \sin^2\phi \gamma(Q) N.
\end{aligned}$$

The mean field parameters are the amplitude S, the angle ϕ and the incommensurate momentum $\vec{Q} = (Q_x, Q_y, Q_z)$; z is the coordination number. The corresponding saddle point equations are obtained from the free energy, determined from

$$\mathcal{F} = -T \sum_k \sum_{\alpha=\pm} \log(1 + \mathrm{e}^{-E_\alpha(k)/T}) + \mu(1-\delta)N + E_0, \tag{9}$$

with E_α equal to

$$E_\alpha = \frac{\epsilon_\uparrow(k+Q) + \epsilon_\downarrow(k)}{2} + \frac{\alpha}{2}\sqrt{[\epsilon_\uparrow(k+Q) - \epsilon_\downarrow(k)]^2 + 4\bar{\Delta}^2} \tag{10}$$

and are given in the appendix (the incommensurate momentum $\vec{Q} = (Q_x, Q_y, Q_z)$ is also determined from a saddle point equation).

We note that incommensurate spiral order in the xy plane leads to a well defined mean field theory, since it is possible to define a close set of equations of motion for the Green functions. Conversely, this is not possible for incommensurate states in the zx or zy planes (in a magnetic field). Due to symmetry, the incommensurate states can only be of the form (Q, Q, Q), (Q, Q, π), and (Q, π, π). In table 1 we show the effect of the doping δ on the incommensurate (Q, Q, Q) and (Q, π, π) wavevectors. It is clear from table 1 that the free energy for the three states (Q, Q, Q), (Q, Q, π), and (Q, π, π) should be essentially the same, and therefore the value of $\mathcal{F}(Q, Q, \pi)$ is not presented.

It is clear from table 1 that the incommensurate spiral phase has a lower free energy for moderate doping. As the doping is reduced the system finds the commensurate phase energetically favourable[1,2]. A detailed evolution, as a function of doping and Δ, of the

[1] The mean field equations have been solved with a 10^{-8} tolerance. From table 2 it is clear that for $N = 80$ and 100 the free energy has the same value up to 9 decimal places. This shows that our results are not N dependent.

[2] The smallness of the energy difference between the commensurate and incommensurate states raises the question about what state will actually be observed in a real material characterized by such a small energy difference. In our opinion, such a material would present coexistence of macroscopic domains where some of the spins either order in a commensurate or incommensurate state (as in an ordinary ferromagnet we have different ferromagnetic domains). However we stress that the observation of the SF state, either in a commensurate or incommensurate state, is not in question.

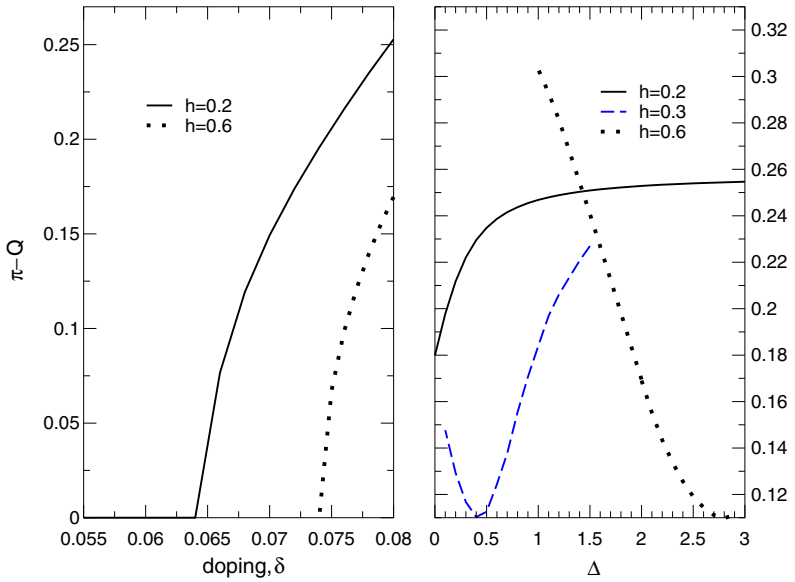

Figure 2. The effect of doping and Δ on the value of the incommensurate momentum, for $T = 0.002$ (temperature in units of t). The t, t', and J parameters are those of table 1, and in the left panel $h = 0.2$, 0.6 and $\Delta = 2$; in the right panel $n = 0.92$ ($\delta = 0.08$) and $h = 0.2$, 0.3, 0.6. Please note that the scanning on δ for $h = 0.2$, corresponds to the second column of table 1.

Table 1. Free energy values for incommensurate momentum Q as a function of density, for $T = 0.002$, $h = 0.2$, $\Delta = 2$. Here and in the remaining figures we have used $t = 1$, $t' = 0.1$ and $J = 0.1$. These results have been obtained in a lattice of $100 \times 100 \times 100$.

δ	$\mathcal{F}(\pi, \pi, \pi)$	Q	$\mathcal{F}(Q, Q, Q)$	Q	$\mathcal{F}(Q, \pi, \pi)$
0.080	−0.171 08	2.9996	−0.171 14	2.8887	−0.171 15
0.078	−0.167 47	3.0066	−0.167 52	2.9067	−0.167 53
0.076	−0.163 90	3.0142	−0.163 94	2.9258	−0.163 94
0.074	−0.160 37	3.0228	−0.160 41	2.9460	−0.160 40
0.072	−0.156 89	3.0327	−0.156 91	2.9678	−0.156 91
0.070	−0.153 45	3.0448	−0.153 47	2.9924	−0.153 47
0.068	−0.150 07	3.0617	−0.150 07	3.0224	−0.150 07
0.066	−0.146 73	3.0891	−0.146 73	3.0649	−0.146 73
0.064	−0.143 45	π	−0.143 45	π	−0.143 45

Table 2. The parameters are $t = 1.0$, $n = 0.92$, $T = 0.0020$, $J = 0.1$, $\Delta = 2.0$, $h = 0.6$, $t' = 0.1$.

	N				
	20	40	60	80	100
$\mathcal{F}$	−0.238 797 251	−0.238 796 45	−0.238 796 513	−0.238 796 512	−0.238 796 512

incommensurate spiral phase for the momentum (Q, π, π) is presented in figure 2. In this figure we present results for different values of the magnetic field ($h = 0.2$, 0.3, 0.6). The behaviour of Q with Δ is seen to be non-monotonous. For a given value of h, $\pi - Q$ may present a minimum (Q maximum) for a given value of Δ. If h is large (for example, $h = 0.6$), such that as Δ is reduced the SP–P transition-line is crossed, we see Q tends to flow away

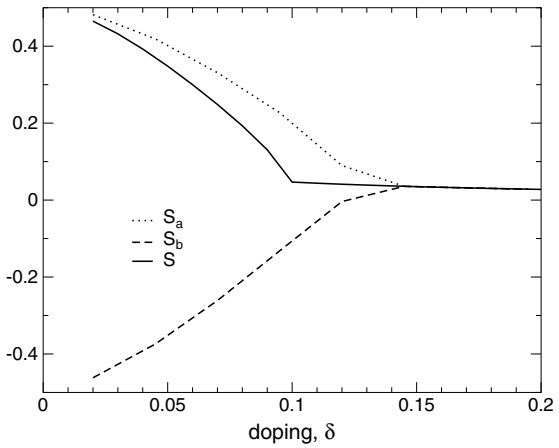

Figure 3. The effect of doping on the magnetic structure at zero temperature. The t, t', and J parameters are those of table 1, and $\Delta = 1.2$ and $h = 0.1$. For these values of the parameters the AF phase is the more stable phase.

from the commensurate π value. In the other cases (for example, $h = 0.3$), Q approaches the commensurate value first ($\pi - Q$ is reduced), reaches the value where $\pi - Q$ is minimum, and starts to deviate again from the commensurate value ($\pi - Q$ increases). (In the P phase there is no meaning for the incommensurate or commensurate states.)

3. Phase diagram at zero and finite temperatures

At $T = 0$ and $\delta = 0$ it is a simple exercise to obtain an analytical solution for the phase diagram of the system. There is no spiral order and the paramagnetic (E_{P}), AF (E_{AF}), and spin flop (E_{SF}) energies are given (for spin $1/2$) by

$$E_{\mathrm{P}} = \tfrac{1}{4} J z \Delta - h, \qquad E_{\mathrm{AF}} = -\frac{J z \Delta}{4}, \tag{11}$$

and

$$E_{\mathrm{SF}} = -\frac{J z}{4} - \frac{h^2}{J z (1 + \Delta)}, \tag{12}$$

respectively. At zero temperature the average value of S, S_A, and S_B is $1/2$. From results (11) and (12) the zero temperature phase diagram of the system can be obtained. The line separating the AF and SF phases is given by $h = zJ\sqrt{\Delta^2 - 1}/2$, and the SF and P phases are separated by the line $h = zJ(\Delta + 1)/2$. When we dope the antiferromagnet, there is a reduction of the average values of S, S_A, and S_B relative to $1/2$, even at zero temperature, as can be seen from figure 3. This behaviour is well known for the 2D isotropic t–t'–J model, and has been used to explain, at the mean field level, the reduction of the Néel temperature in high-temperature superconductors, upon doping. Here, the presence of the magnetic field combined with doping forces the AF phase to a ferrimagnetic phase, where the average value of spin in the two sublattices is not the same even at zero temperature. This is in contrast to the pure Heisenberg case, where $S_A = S_B = 1/2$ at zero temperature in the presence of h. Upon increasing doping, the average values of S, S_A, and S_B are reduced to the paramagnetic value, fixed by the magnetic field. Above a given value of δ, there is no magnetic order in the ground state of the system, and its behaviour is that of a collection of fully polarized independent electrons.

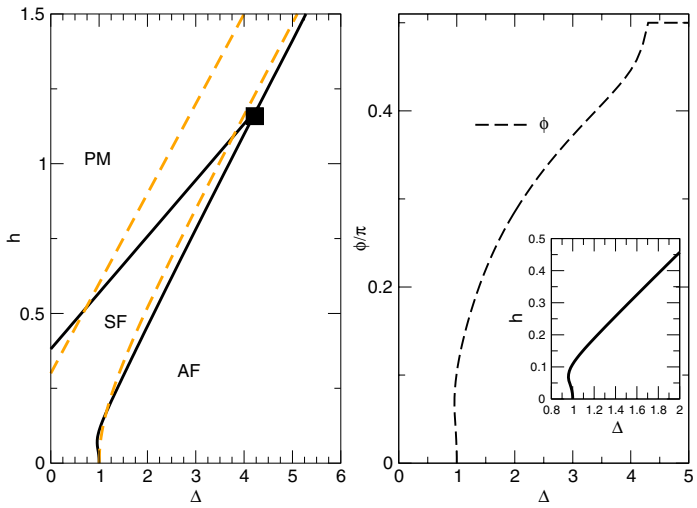

Figure 4. Left panel: zero temperature phase diagram of the 3D t–t'–J model, for $1-\delta = n = 0.92$. The t, t', and J parameters are those of table 1. The black box marks the point where the first-order AF–SF and the second-order SF–PM transition lines meet. For values of Δ above the black box there is a AF–PM second-order transition line only. The pure Heisenberg phase diagram is represented by the dashed lines. The full curves represent the phase diagram for the doped case. Right panel: variation of the SF angle ϕ, in units of π, along the AF–SF transition line. The inset shows the phase diagram close to $\Delta = 1$. A minute reentrant behaviour is seen.

This reduction of S, S_A, and S_B together with the combined effect of Δ and h has consequences for the zero temperature phase diagram of the doped antiferromagnet, when compared with the pure Heisenberg case discussed above. The picture is the following: doping introduces holes here and there in the lattice and as consequence some of the magnetic interactions due to the Heisenberg term cannot be fulfilled; as a consequence, and for a given $\Delta > 1$, as the magnetic field increases, the system finds it favourable to take advantage of the Zeeman energy and therefore the first-order AF–SF transition should occur at a lower value of h; for the same reason, the SF phase cannot fulfill all the AF interactions in the xy plane, and therefore the second-order SF–P transition should also occur at lower values of h.

This picture is confirmed by the phase diagram shown in figure 4. In this figure, and for Δ roughly in the range $1 < \Delta < 4$, we see that both the first-order AF–SF and the second-order SF–P transition lines are pulled down to lower values of h relative to the pure Heisenberg case. Furthermore, and in contrast to the pure Heisenberg case, the SF phase does not span an infinite area in the (Δ, h) plane. There is a point where the second-order SP–P line meets the first-order AF–SF line (represented by a black square in figure 4). From this point on we are left with an AF–P second-order transition; below this line the spins in the AF phase are fully aligned with the field, but have different magnitudes for the two sub-lattices. For values of $\Delta < 1$ the system finds it preferable to be in the SF phase. We note that in figure 4 the spin flop phase is of incommensurate type, in agreement with the results of figure 2. In fact using figure 2 in connection with the phase diagram of figure 4 it is possible to see the evolution of the incommensurate momentum Q over the phase diagram.

We can now ask, how do the transition lines change with doping? This question has experimental relevance in connection to measured spin flop fields in $La_{2-x}Sr_xCuO_4$ [19], where it was found that the critical field for the SF transition is reduced upon doping. In figure 5 we show both the effect of δ on the SF–P line, for small values of Δ (left panel), and on the AF–SF

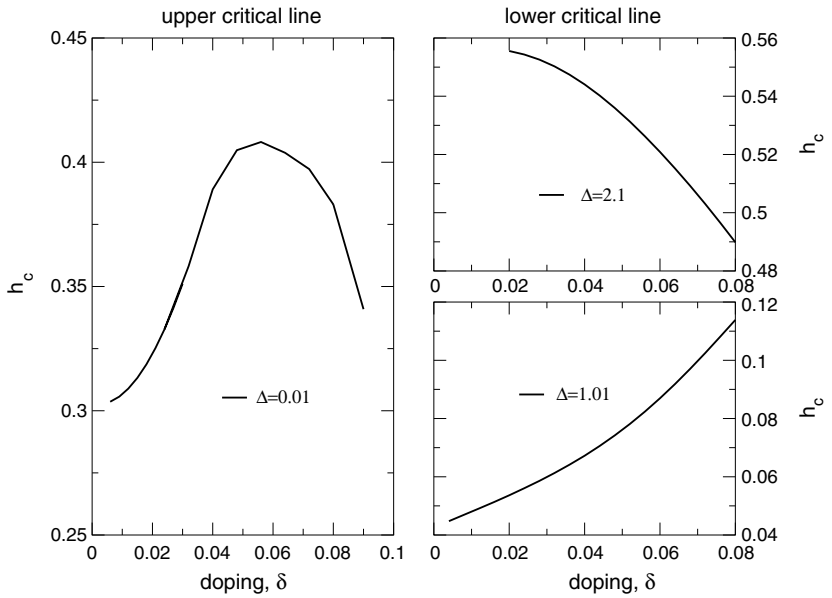

Figure 5. The effect of doping on the critical field h_c. In the left panel we show the effect of δ on the SF–P transition, close to the $\Delta = 0$ case. The right panel shows the value of the critical field h_c for the AF–SF transition for two values of Δ. The t, t', and J parameters are those of table 1.

line for two values of Δ. We see that for values of the exchange $\Delta = 2$ there is a reduction of h_c upon doping (we remark that this behaviour is not restricted to the single value $\Delta = 2$, but it exists over a finite range of Δ-values). On the other hand, the effect for values such that $\Delta \sim 1$ is to introduce an increase of h_c. Although our calculation cannot be extended quantitatively to $La_{2-x}Sr_xCuO_4$ mainly because the spin flop transition in this material is due to the Dzyaloshinskii–Moriya interaction, we do not expect qualitative changes in regard to the behaviour of h_c with doping [24][3]. That is, it is possible to account at the mean field level for the decrease of h_c with doping, independently of the details of the interaction, as long as an AF–SF transition exists.

Let us see now how the zero-temperature picture evolves when we extend the analysis to finite temperatures. Since the Bose–Einstein condensation temperature is of the order of the doping, $T_{BE} \sim \delta t$, we can draw a finite temperature phase diagram using the same formulation we used for zero T as long as $T < T_{BE}$. We have stayed in this regime. As for the pure Heisenberg case, we obtain a bicritical point where the first-order AF–SF transition line meets the two second-order lines, describing the AF–P and the SF–P transitions. Comparing with the pure case, the main changes are:

(i) the bicritical point (T_b, h_b) moves to lower temperatures;
(ii) the SF region shrinks as we dope the system up to a point where only the AF and the P phases remain (the area of the AF zone is also reduced).

The disappearance of the SF phase with doping before the AF phase is related to the zero temperature dependence of the average value S upon doping that is seen in figure 3, where the S attains its paramagnetic value before the S_A and S_B do so. The aspects discussed above are

[3] The Dzyaloshinskii–Moriya interaction $\sum_{i,j} \vec{D} \cdot (\vec{S}_i \times \vec{S}_j)$ is responsible for two effects: (i) a canting of the spins from the CuO_4 planes, and (ii) a SF transition when a magnetic field is applied perpendicular to the CuO_4 planes.

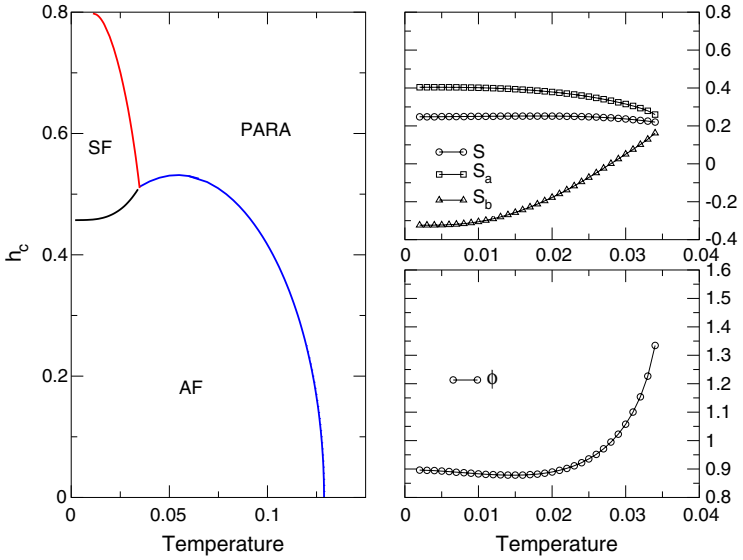

Figure 6. Finite temperature phase diagram of the 3D t–t'–J model, for $\Delta = 2$ and $1 - \delta = n = 0.92$. The t, t', and J parameters are those of table 1. The left panel shows the phase diagram, and the right panels show S, S_A, S_B, and ϕ as function of T along the AF to SP first-order transition line.

shown in figure 6, where in the left panel the phase diagram is depicted, and in the right one we plot the dependence of the average values of S, S_A, and S_B, and the angle ϕ in the SF phase along the first-order AF–SF transition line. We see that close to the bicritical point, and in a reduced range of temperatures, the angle ϕ has a fast variation. Therefore, for an experiment probing the AF–SF transition with temperature, at different fields close to the bicritical point we may see a large or small jump in the magnetization, depending on the field strength. Such a behaviour could be easily observed by performing magnetization measurements of the type presented for $La_{2-x}Sr_xCuO_4$ [19], but with the magnetic field applied along the CuO_4 planes. Again, our discussion of the relation between our findings and the experimental results in $La_{2-x}Sr_xCuO_4$ applies with the limitations discussed above.

4. Characterization of the spin flop phase

Let us characterize the metallic SF phase. We consider both magnetic and charge transport properties. We first compute the magnetic longitudinal and transverse susceptibility. We then study the optical conductivity, computing both the Drude weight and the regular part of the conductivity.

4.1. Magnetic susceptibility

The dynamic magnetic susceptibility, $\chi_{\alpha,\beta}(q, i\omega_n)$, is defined as

$$\chi_{\alpha,\beta}(q, i\omega_n) = \int_0^\beta d\tau \, e^{-i\omega_n \tau} \langle T S_\alpha(q, \tau) S_\beta(-q, 0) \rangle, \tag{13}$$

where

$$S_\mu(q) = \frac{1}{2N}\sum_{k,\alpha,\beta} f^\dagger_{k+q,\alpha}\sigma^{(\alpha,\beta)}_\mu f_{k,\alpha}. \tag{14}$$

In the SF phase we can define four types of Green functions, generically written as

$$G_{\alpha,\beta}(k,\, p,\, \tau) = -\langle T f_{k,\alpha}(\tau) f^\dagger_{p,\beta}(0)\rangle. \tag{15}$$

For each case the results in the Matsubara representation are

$$G_{\uparrow,\uparrow}(k,\, p,\, \mathrm{i}\omega_n) = \frac{\delta_{k,p}[\mathrm{i}\omega_n - \epsilon_\downarrow(k-Q)]}{[\mathrm{i}\omega_n - \epsilon_\downarrow(k-Q)][\mathrm{i}\omega_n - \epsilon_\uparrow(k)] - \bar{\Delta}^2},$$

$$G_{\downarrow,\uparrow}(k,\, p,\, \mathrm{i}\omega_n) = \frac{\bar{\Delta}G_{\uparrow,\uparrow}(k+Q,\, p,\, \mathrm{i}\omega_n)}{\mathrm{i}\omega_n - \epsilon_\downarrow(k)},$$

$$G_{\downarrow,\downarrow}(k,\, p,\, \mathrm{i}\omega_n) = \frac{\delta_{k,p}[\mathrm{i}\omega_n - \epsilon_\uparrow(k+Q)]}{[\mathrm{i}\omega_n - \epsilon_\downarrow(k)][\mathrm{i}\omega_n - \epsilon_\uparrow(k+Q)] - \bar{\Delta}^2},$$

$$G_{\uparrow,\downarrow}(k,\, p,\, \mathrm{i}\omega_n) = \frac{\bar{\Delta}G_{\downarrow,\downarrow}(k-Q,\, p,\, \mathrm{i}\omega_n)}{\mathrm{i}\omega_n - \epsilon_\uparrow(k)}.$$

Since $G_{\uparrow,\uparrow}(k,\, p,\, \mathrm{i}\omega_n)$ and $G_{\downarrow,\downarrow}(k,\, p,\, \mathrm{i}\omega_n)$ are diagonal in momentum space, the only non-zero off-diagonal Green functions in spin space are $G_{\downarrow,\uparrow}(p-Q,\, p,\, \mathrm{i}\omega_n)$ and $G_{\uparrow,\downarrow}(p+Q,\, p,\, \mathrm{i}\omega_n)$.

At the mean field level, the longitudinal magnetic susceptibility, $\chi_{z,z}$, and the transverse magnetic susceptibility, $\chi_{-,+}$, are obtained using the definition (13) combined with the Green functions (15). The general form of the susceptibility is

$$\chi_{\alpha,\beta}(q, \mathrm{i}\omega_n) = -\frac{1}{N}\sum_p \sum_{i,l=1}^{2} T[E_j(p+q),\, E_l(p),\, \mathrm{i}\omega_n][M_{j,l,\alpha,\beta}(p,q)]^2, \tag{16}$$

where

$$T[E_j(p+q),\, E_l(p),\, \mathrm{i}\omega_n] = \frac{f[E_j(p+q)] - f[E_l(p)]}{\mathrm{i}\omega_n + E_j(p+q) - E_l(p)}, \tag{17}$$

and

$$M_{j,l,z,z}(p,q) = \tfrac{1}{2}[R_{\uparrow,j}(p+q)R_{\uparrow,l}(p) - R_{\downarrow,j}(p+q)R_{\downarrow,l}(p)], \tag{18}$$

$$M_{j,l,-,+}(p,q) = R_{\downarrow,j}(p+q)R_{\uparrow,k}(p-Q). \tag{19}$$

Here $f(x) = (1+\mathrm{e}^{x/T})^{-1}$ and the $R_{\alpha,j}$ factors are given in the appendix.

The behaviour of $\chi_{z,z}(0,0)$ and $\chi_{-,+}(0,0)$ is presented in figure 7. Above the SF–P transition line defined by the phase diagram of figure 6, the behaviour of the susceptibility is that of a paramagnet in a magnetic field. As $h \to 0$, $\chi_{+-} = 2\chi_{zz}$. Below the transition temperature, there is a sudden drop in the magnetic susceptibility, followed by the same abrupt behaviour of the SP angle ϕ. As the temperature is further reduced the susceptibility shows an upturn at low temperature, which is typical of the susceptibility of metallic antiferromagnets, as in the case of Pt_3Fe [25].

4.2. Optical conductivity

The response of the system to an electromagnetic field is obtained from the optical conductivity. This quantity is defined as [26]

$$\sigma_{xx}(\vec{q}, \omega) = \frac{1}{N}\frac{\langle K_{xx}\rangle + \Lambda_{xx}(\vec{q}, \omega)}{\mathrm{i}(\omega + \mathrm{i}0^+)}, \tag{20}$$

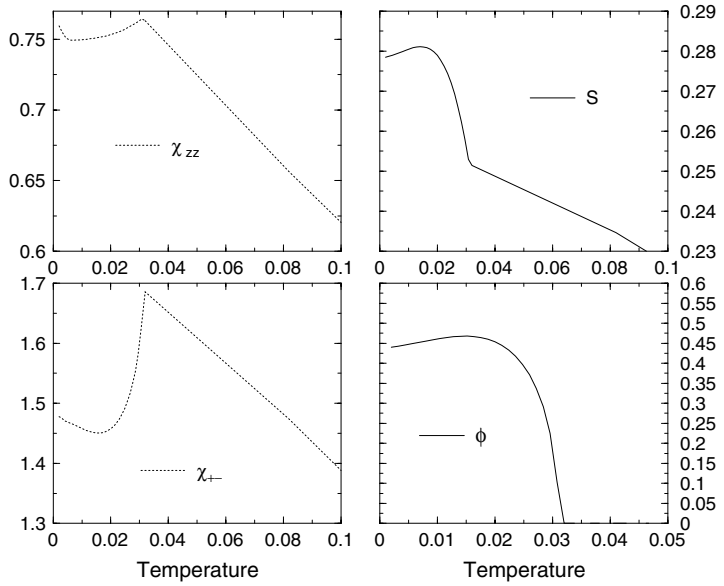

Figure 7. Spin susceptibility $\chi_{z,z}(0,0)$ and $\chi_{-,+}(0,0)$ at finite temperature in the SF region of the phase diagram for $\Delta = 2$, $h = 0.6$ and $n = 0.92$. The t, t', and J parameters are those of table 1.

where $\Lambda_{xx}(\vec{q},\omega)$ is the retarded current–current correlation function, obtained from the corresponding Matsubara correlation function

$$\Lambda_{xx}(\vec{q},\mathrm{i}\omega_n) = \int_0^\beta \mathrm{d}\tau\, \mathrm{e}^{\mathrm{i}\omega_n\tau}\langle T_\tau j_x^p(\vec{q},\tau) j_x^p(-\vec{q},0)\rangle, \tag{21}$$

and K_{xx} is given by

$$K_{xx} = \sum_k e(k+Q) f^\dagger_{\uparrow,k+Q} f_{\uparrow,k+Q} + e(k) f^\dagger_{\downarrow,k} f_{\downarrow,k}. \tag{22}$$

Here $e(k) = -2t\delta\cos q_x - 4t'\delta\cos q_x(\cos q_y + \cos q_z)$ and $j_x^p(\vec{q})$ is a Fourier component of the current operator [26]. Writing $\sigma(\vec{q},\omega) = \sigma'(\vec{q},\omega) + \mathrm{i}\sigma''(\vec{q},\omega)$, that is, separating the real and imaginary parts, the real part reads

$$\begin{aligned}\sigma'(\vec{q},\omega) &= -\frac{\pi}{N}\delta(\omega)[\langle K_{xx}\rangle + \Lambda'_{xx}(\vec{q},\omega)] + \frac{\Lambda''_{xx}(\vec{q},\omega)}{N\omega} \\ &= \pi\delta(\omega)D + \sigma_{\mathrm{reg}}(\vec{q},\omega),\end{aligned} \tag{23}$$

where D is the charge stiffness or Drude weight, given by

$$D = -\frac{1}{N}[\langle K_{xx}\rangle + \Lambda'_{xx}(0,0)]. \tag{24}$$

The zero momentum conductivity is given by

$$\sigma_{\mathrm{reg}}(\omega) = \frac{\Lambda''_{xx}(0,\omega)}{N\omega} = \pi\sum_p \sum_{m\neq j=1}^{2} M_{m,j}\delta(\omega + E_j - E_m), \tag{25}$$

with

$$\begin{aligned}M_{m,j} = [f(E_j) - f(E_m)][&j^2(p+Q)R^2_{\uparrow,m}R^2_{\uparrow,j} + 2j(p+Q)j(p) \\ &+ R_{\uparrow,m}R_{\uparrow,j}R_{\downarrow,m}R_{\downarrow,j} + j^2(p)R^2_{\downarrow,m}R^2_{\downarrow,j}],\end{aligned} \tag{26}$$

where $j(k) = 2t\delta\sin q_x + 4t'\delta\sin q_x(\cos q_y + \cos q_z)$.

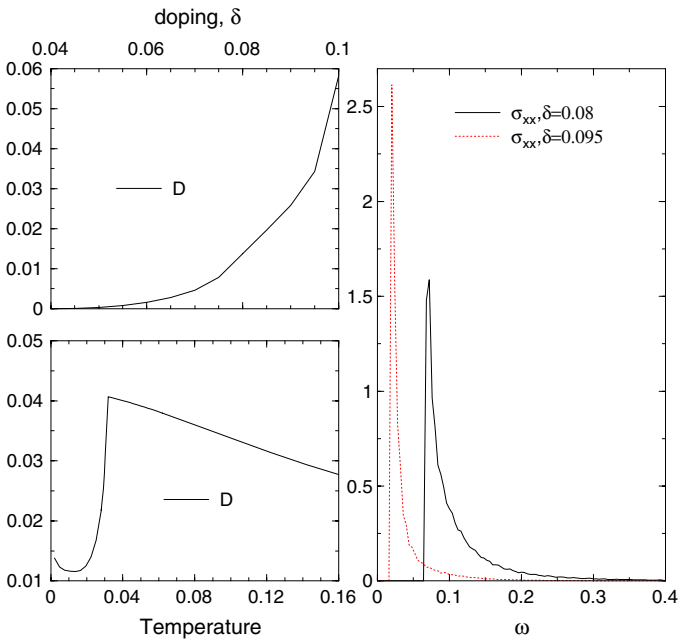

Figure 8. Optical conductivity and Drude weight of the 3D t–t'–J model, for $\Delta = 2$ and $n = 0.92$, $h = 0.6$. The t, t', and J parameters are those of table 1. In the left panels we show the effect of the doping on the zero temperature Drude weight, D, and the effect of the temperature on D as the SF–P transition line is crossed. In the right panel, the regular part $\sigma_{\rm reg}$ of the optical conductivity is depicted.

A finite Drude weight establishes an infinite dc conductivity. If the system is an insulator D is zero. On the other hand, $\sigma_{\rm reg}(\omega)$, establishes the absorption of finite frequency light by the system. In figure 8 we show the effect of the doping and of the temperature on D, as well as the effect of the doping on $\sigma_{\rm reg}(\omega)$ at zero temperature. At zero temperature we realize that the effect of increasing δ is two fold: (i) it increases D (more carriers available); (ii) it shifts $\sigma_{\rm reg}(\omega)$ to lower values in frequency, because the gap decreases with δ. When $\delta \to 0$, both D and $\sigma_{\rm reg}(\omega)$ vanish. We expect this result to hold beyond our mean field analysis [27]. At finite temperature and constant δ, there are two situations. Above the SF–P transition the Drude weight exhausts the sum rule obeyed by $\sigma(\omega)$, and therefore there is no finite energy absorption. When the SF–P transition line is crossed, there is a reduction of D, with a transfer of spectral weight to finite energies. The diminishing of D is quite abrupt in a small range of temperatures, and this fact opens the possibility of having a large magneto-resistance in these systems, when scattering from impurities is included.

5. Conclusions

In conclusion, we have, in this paper, described the mean field theory of SF transitions in doped antiferromagnets. Furthermore, we have characterized the SF phase from the point of view of its magnetic and charge-transport properties. We have shown that the AF phase is characterized by a field-induced ferrimagnetic ground state, at odds with the pure Heisenberg case, and that a SF phase exists in a finite range of Δ and h. The Drude weight of the system was shown to present an abrupt decrease in a reduced range of temperatures when the system

enters the SF phase, and a similar behaviour occurs with the magnetic susceptibility. We have also studied the behaviour of the critical lines with doping, and found that depending on the value of Δ the critical field associated with the AF–SF transition-line may increase ($\Delta \sim 1$) or decrease ($\Delta > 1$) with the doping δ. We have also shown that the behaviour of the critical field associated with the SF to P transition is non-monotonous with δ. Although the full magnetic behaviour of doped La_2CuO_4 in a magnetic field cannot be quantitatively described by an antiferromagnet with an anisotropic exchange, since the origin of the SF phase in this material is due to the Dzyaloshinskii–Moriya interaction, we believe that some of the above qualitative findings still apply. The main reason, we believe, is the fact that some physical properties will not depend so much on the details of the interaction but on the existence of a physical mechanism allowing for a spin flop transition. Only this reasoning may explain why the upper right panel of figure 6 exhibits a decreasing of the lower critical field with doping, as observed in doped La_2CuO_4. Also the existence of an incommensurate spin flop phase will not depend on the detail of the interaction but only on the competition between the kinetic and interaction energies. The reason why an incommensurate spin flop state is not observed in pure La_2CuO_4 is precisely the absence of the kinetic energy term. On the contrary, details such as the line borders separating the different phases, the values of the incommensurate momentum and the amount of reduction of the critical field with doping will certainly be interaction dependent.

Acknowledgments

The author thanks J M B Lopes dos Santos for many discussions about critical points and phase transitions, and P D Sacramento and J L Ribeiro for carefully reading the manuscript and suggestions.

Appendix. Green function decomposition, mean field equations and susceptibility

In the spin flop phase all the Green functions can be cast in the form

$$G_{\alpha,\beta}(p, \mathrm{i}\omega_n) = \sum_{j=1}^{2} \frac{R_{\alpha,j} R_{\beta,j}}{\mathrm{i}\omega_n - E_j}. \tag{A.1}$$

In particular we have that

$$G_{\uparrow,\uparrow}(p+Q, \mathrm{i}\omega_n) = \sum_{j=1}^{2} \frac{[R_{\uparrow,j}(p)]^2}{\mathrm{i}\omega_n - E_j(p)},$$

$$G_{\downarrow,\downarrow}(p, \mathrm{i}\omega_n) = \sum_{j=1}^{2} \frac{[R_{\downarrow,j}(p)]^2}{\mathrm{i}\omega_n - E_j(p)},$$

$$G_{\downarrow,\uparrow}(p, p+Q, \mathrm{i}\omega_n) = \sum_{j=1}^{2} \frac{R_{\downarrow,j}(p) R_{\uparrow,j}(p)}{\mathrm{i}\omega_n - E_j(p)},$$

$$G_{\uparrow,\downarrow}(p+Q, p, \mathrm{i}\omega_n) = \sum_{j=1}^{2} \frac{R_{\downarrow,j}(p) R_{\uparrow,j}(p)}{\mathrm{i}\omega_n - E_j(p)},$$

where the coherence factors are

$$[R_{\uparrow,1}(p)]^2 = [R_{\downarrow,2}(p)]^2 = \frac{1}{2}\left(1 + \frac{\epsilon_\downarrow(p) - \epsilon_\uparrow(p+Q)}{\sqrt{\alpha(p)}}\right),$$
$$1 = \sum_{j=1}^{2}[R_{\alpha,j}(p)]^2, \tag{A.2}$$
$$R_{\downarrow,1}(p)R_{\uparrow,1}(p) = -R_{\downarrow,2}(p)R_{\uparrow,2}(p) = -\frac{\bar{\Delta}}{\sqrt{\alpha(p)}},$$

with $\alpha(p) = [\lambda(p)]^2 + 4\bar{\Delta}^2$ and $\lambda(p) = \epsilon_\uparrow(p+Q) - \epsilon_\downarrow(p)$.

The mean field equations can be expressed in terms of the coherence factors as

$$1 - \delta = \frac{1}{N}\sum_k \sum_{j=1}^{2}(R_{\uparrow,j}^2 + R_{\downarrow,j}^2) f(E_j), \tag{A.3}$$

$$S\sin(2\phi)[\Delta z - \gamma(Q)] = -\gamma(Q)\cos\phi\frac{1}{N}\sum_k\sum_{j=1}^{2}2R_{\uparrow,j}R_{\downarrow,j}f(E_j)$$
$$+ \Delta z\sin\phi\frac{1}{N}\sum_k\sum_{j=1}^{2}(R_{\uparrow,j}^2 - R_{\downarrow,j}^2)f(E_j), \tag{A.4}$$

$$S[z\Delta\cos^2\phi + \gamma(Q)\sin^2\phi] = \Delta z\cos\phi\frac{1}{2N}\sum_k\sum_{j=1}^{2}(R_{\uparrow,j}^2 - R_{\downarrow,j}^2)f(E_j)$$
$$+ \gamma(Q)\sin\phi\frac{1}{2N}\sum_k\sum_{j=1}^{2}2R_{\uparrow,j}R_{\downarrow,j}f(E_j). \tag{A.5}$$

The above equations hold for both the commensurate and incommensurate cases. In the incommensurate case an additional equation is required for the determination of Q_j ($j = x, y, z$)—the incommensurate momentum value. This equation reads

$$\frac{\partial\mathcal{F}}{\partial Q_j} = 0 \Leftrightarrow \frac{1}{N}\sum_k\sum_{\alpha=\pm}\frac{\partial E_\alpha}{\partial Q_j}f(E_\alpha) + JS^2\sin^2\phi\sin Q_j = 0. \tag{A.6}$$

The partial derivatives of the quasi-particle dispersions E_α are straightforward but give long equations we omit here.

The full expression for the $\chi_{zz}(0,0)$ susceptibility useful for any value of the doping δ is given by

$$\chi_{zz}(0,0) = -\sum_{k,\alpha=\pm}\alpha f(E_\alpha)\frac{2\bar{\Delta}^2}{[\alpha(k)]^{3/2}} + \sum_{k,\alpha=\pm}\frac{1}{4}\frac{[\lambda(k)]^2 f(E_\alpha)f(-E_\alpha)}{T\alpha(k)}. \tag{A.7}$$

References

[1] Shapira Y and Foner S 1970 *Phys. Rev.* B **1** 3083
[2] Schweika W, Maleyev S V, Brückel Th and Plakhty V P 2002 *Europhys. Lett.* **60** 446
[3] Birgeneau R J, Shirane G, Blumet M and Koehler W C 1974 *Phys. Rev. Lett.* **33** 1098
[4] Rohrer H and Gerber Ch 1977 *Phys. Rev. Lett.* **38** 909–12
[5] Néel L 1936 *Ann. Phys. Fr.* **5** 232
[6] Anderson F B and Callen H B 1964 *Phys. Rev.* **136** A1068
[7] Feder J and Pytte E 1968 *Phys. Rev.* **168** 168
[8] Fisher M E and Nelson D R 1974 *Phys. Rev. Lett.* **32** 1350
[9] Kohno M and Takahashi M 1997 *Phys. Rev.* B **56** 3212

[10] Yunoki S 2002 *Phys. Rev.* B **65** 092402
[11] Schmid G, Todo S, Troyer M and Dorneich A 2002 *Phys. Rev. Lett.* **88** 167208
[12] Peres N M R and Sandvik A 2002 unpublished (The calculation used the cluster of GCEP, at the University of Minho)
[13] Matsubara T and Matsuda H 1956 *Prog. Theor. Phys.* **16** 569
Matsuda H and Tsuneto T 1970 *Prog. Theor. Phys. Suppl.* **46** 411
[14] Bernardet K, Batrouni G G, Meunier J-L, Schmid G, Troyer M and Dorneich A 2002 *Phys. Rev.* B **65** 104519
[15] Greiner M, Mandel O, Esslinger T, Hänsch T and Bloch I 2002 *Nature* **415** 39
[16] See Batrouni G G, Rousseau V, Scalettar R T, Rigol M, Muramatsu A, Denteneer P J H and Troyer M 2002 *Phys. Rev. Lett.* **89** 117203 and references therein
[17] Lee J-W, Cha M-C and Kim D 2001 *Phys. Rev. Lett.* **87** 247006
Lee J-W, Cha M-C and Kim D 2002 *Phys. Rev. Lett.* **88** 049901
[18] Jayaprakash C, Krishnamurthy H R and Sarker S 1989 *Phys. Rev.* B **40** 2610
[19] Suzuki T, Goto T, Chiba K, Fukase T, Fujita M and Yamada K 2002 *Phys. Rev.* B **66** 172410
[20] Thio T, Thurston T R, Preyer N W, Picone P J, Kastner M A, Jenssen H P, Gabbe D R, Chen C Y, Birgeneau R J and Aharony A 1988 *Phys. Rev.* B **38** 905
[21] Ivanov M A, Loktev V M and Pogorelov Yu G 1992 *Zh. Eksp. Teor. Fiz.* **101** 596
[22] Held K, Ulmke M, Blümer N and Vollhardt D 1997 *Phys. Rev.* B **56** 14469
[23] Coleman P 1984 *Phys. Rev.* B **29** 3035
[24] de Castro E V, Peres N M R and Lopes dos Santos J M B, in preparation
See also Fairall C W and Cowen J A 1970 *Phys. Rev.* B **2** 4636 on the classical Heisenberg Hamiltonian
[25] Crangle J 1991 *Solid State Magnetism* (London: Edward Arnold) p 117
[26] Mahan G D 2000 *Many-Particle Physics* 3rd edn (Dordrecht: Kluwer–Plenum) p 173
[27] Côté R and Trembley A-M S 1995 *Europhys. Lett.* **20** 37